Magnetic Fluctuation Power Near Proton Temperature Anisotropy Instability Thresholds in the Solar Wind

S. D. Bale,[1] J. C. Kasper,[2] G. G. Howes,[3] E. Quataert,[4] C. Salem,[5] and D. Sundkvist[5]

[1]*Physics Department and Space Sciences Laboratory, University of California, Berkeley, California, USA*
[2]*Harvard-Smithsonian Center for Astrophysics, Cambridge, Massachusetts, USA*
[3]*Department of Physics and Astronomy, University of Iowa, Iowa City, Iowa, USA*
[4]*Physics Department and Astronomy Department, University of California, Berkeley, California, USA*
[5]*Space Sciences Laboratory, University of California, Berkeley, California, USA*
(Received 9 August 2009; published 16 November 2009)

The proton temperature anisotropy in the solar wind is known to be constrained by the theoretical thresholds for pressure-anisotropy-driven instabilities. Here, we use approximately 1×10^6 independent measurements of gyroscale magnetic fluctuations in the solar wind to show for the first time that these fluctuations are enhanced along the temperature anisotropy thresholds of the mirror, proton oblique firehose, and ion cyclotron instabilities. In addition, the measured magnetic compressibility is enhanced at high plasma beta ($\beta_\parallel \gtrsim 1$) along the mirror instability threshold but small elsewhere, consistent with expectations of the mirror mode. We also show that the short wavelength magnetic fluctuation power is a strong function of collisionality, which relaxes the temperature anisotropy away from the instability conditions and reduces correspondingly the fluctuation power.

The physical processes that regulate the expansion of the super-Alfvénic solar wind into space include adiabatic particle motion, plasma instabilities, and binary particle collisions. As the wind expands, plasma density n_p and magnetic field $|B|$ decrease radially. The Chew-Goldberger-Low (CGL) relations [1] predict that the plasma ions should become anisotropic in the sense of $T_\parallel > T_\perp$ if the particle motion is adiabatic and collisionless; here, T is the ion temperature parallel and perpendicular to the background magnetic field. However, Coulomb collisions and pressure-anisotropy instabilities act to pitch-angle scatter the plasma back towards isotropy [2]. At 1 AU, the measured most probable value of the proton temperature anisotropy is $T_\perp/T_\parallel \approx 0.89$ (Fig. 1, top panel below). If CGL were valid, this would imply a proton temperature anisotropy of $T_\perp/T_\parallel \gtrsim 200$ at 5 solar radii.

The same pressure-anisotropy instabilities that operate in the solar wind are believed to operate in other low-collisionality astrophysical plasmas, including clusters of galaxies [3] and some accretion disks onto black holes [4,5]. In the latter environment, these instabilities not only modify the thermodynamics of the plasma (as in the solar wind), but they also play a crucial dynamical role, regulating the anisotropic stress that helps transport angular momentum, allowing accretion to proceed.

Growth of ion temperature anisotropy instabilities has been studied in a (relatively collisional) laboratory device, where isotropization and magnetic fluctuations were observed corresponding to the Alfvén ion cyclotron instability [6]. Similar results were obtained in the solar wind at 1 AU [7] (for $T_\perp/T_\parallel > 1$ and solar wind speeds greater than 600 km/s), suggesting that the proton cyclotron in-

stability plays a role. Both mirror mode and ion cyclotron anisotropy instabilities appear to be active in the terrestrial magnetosheath, inferred from observed constraints on the temperature anisotropy [8,9].

Recently, Kasper *et al.* [10] used measurements from the Wind spacecraft to show that the solar wind proton temperature anisotropy $T_\perp/T_\parallel$ is constrained by proton parallel beta $\beta_\parallel [= n_p k_b T_\parallel/(B^2/2\mu_0)]$ in a way that is consistent with expectations of the proton firehose instability (for $T_\perp/T_\parallel < 1$). Hellinger *et al.* (2006) compared linear instability calculations with the measured anisotropies (from this same dataset) and found that the constraints on the observed anisotropies were best described by the mirror instability (in contrast to previous results [7]) for the case of perpendicular anisotropy ($T_\perp/T_\parallel > 1$) and the oblique firehose instability for parallel anisotropy ($T_\perp/T_\parallel < 1$). An instability threshold can be derived by calculating marginal stability (in practice $\gamma = 10^{-3}\omega_{ci}$) for values of $\beta_\parallel$ [11].

$$\frac{T_\perp}{T_\parallel} = 1 + \frac{a}{(\beta_\parallel - \beta_0)^b}. \qquad (1)$$

Equation (1) generalizes previous results [7,12] and constrains the observations for values of a, b, and β_0 corresponding to the mirror and oblique firehose instabilities (coefficients are given below).

Here, we use experiments on the Wind spacecraft to show the first direct correspondence of the measured wave power to the anisotropy-driven instabilities. Wind was launched in 1994 and has spent long intervals in the ambient solar wind. The data set spans the time interval Nov. 21, 1994 to Nov. 12, 2004 and includes 1 026 112
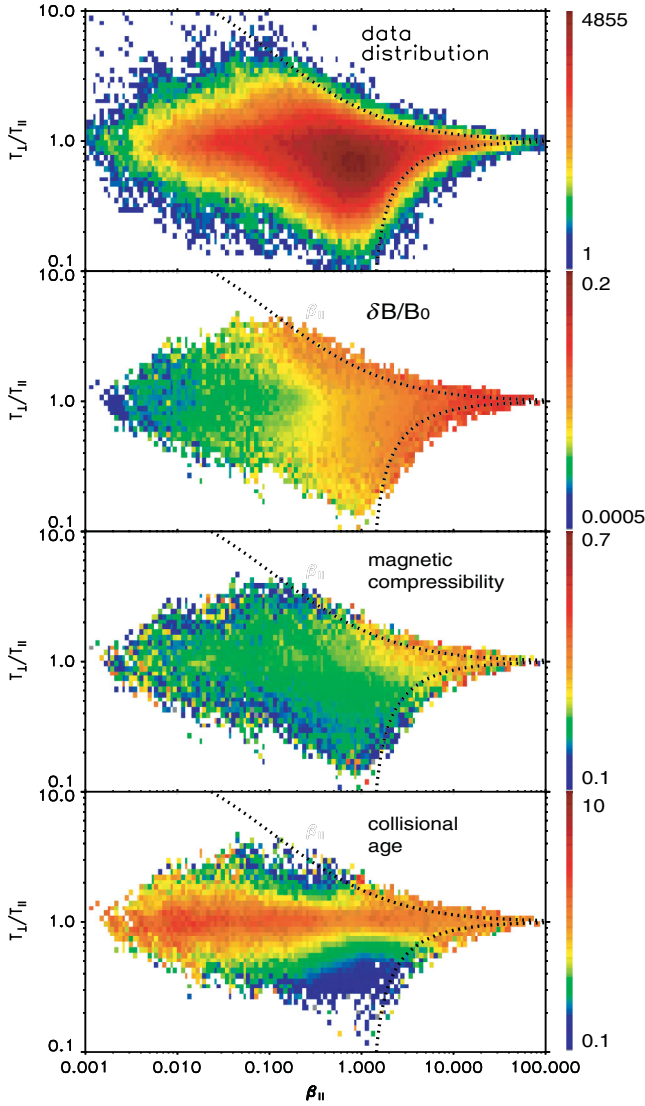
FIG. 1 (color).   The distribution of proton temperature anisot-
ropy ($T_\perp/T_\parallel$) measurements with respect to the parallel plasma
beta $\beta_\parallel$ (upper panel) is constrained by the oblique proton
firehose instability threshold (lower dotted line) and the mirror
instability threshold (upper dotted line). In the second panel, the
magnetic fluctuation amplitude $|\delta B|/|B|$ is shown to be en-
hanced along the instability thresholds and overall at high $\beta_\parallel$
where the thresholds converge. The third panel shows magnetic
compressibility $\delta B_\parallel^2/(\delta B_\parallel^2 + \delta B_\perp^2)$, which is enhanced at high
$\beta_\parallel$ (>1) along the mirror threshold, as expected for the mirror
instability. The lower panel shows the "collisional age," which
is largest around $T_\perp/T_\parallel \approx 1$ suggesting that isotropy results
largely from Coulomb collisions. Anisotropic plasma is rela-
tively collisionless.

independent measurements of solar wind plasma and mag-
netic field. Proton density n_p, velocity $\vec{v}_{sw}$, and tempera-
ture are measured by the Faraday cup instrument of SWE
(solar wind experiment) [13]. Both the parallel proton
temperature $T_\parallel$ and perpendicular temperature $T_\perp$ are
computed by comparison with the average magnetic field

direction. The magnetic field investigation (MFI) is used to
measure the solar wind magnetic field [14] at either 22
vectors/s or 11 vectors/s depending on telemetry mode and
averaged to 3 s intervals; we denote this 3 s average data as
$\vec{B}$. The vector rms fluctuation field during the 3 s average
interval is denoted as $\delta\vec{B}$. Each fluctuation field mea-
surement $\delta\vec{B}$ is rotated into a coordinate system defined
by the average field direction $\hat{B}$ so that we have both the
compressive component $\delta B_\parallel$ and the shear component
$\delta B_\perp[= (\delta B_{\perp,1}^2 + \delta B_{\perp,2}^2)^{1/2}]$. We then define the magnetic
compressibility as $\delta B_\parallel^2/(\delta B_\parallel^2 + \delta B_\perp^2)$ [15]. The magnetic
field is an rms measurement over the bandwidth $\Delta f =
(0.3 - 5.5)$ Hz, or $(0.3 - 11)$ Hz in high TM mode.
Since the magnetic fluctuation spectrum falls as $f^{-5/3}$ (or
steeper) at these frequencies, the power in this bandwidth is
dominated by the lowest measured frequency $f_0 \approx 0.3$ Hz.
Since it is believed that $k_\perp \gg k_\parallel$ [16], the natural frequen-
cies of the turbulence are all much lower than the sample
frequency (i.e., $f_0 \gg f_{ci}$), and Taylor's hypothesis applies
($\omega = kv_{sw}$). Therefore, the measured power at $f_0 \approx
0.3$ Hz corresponds to power at wave number $k\rho_i \approx
(f_0/f_{ci})(v_{th}/v_{sw})$. The distribution (in our data) of this
parameter is sharply peaked at $k\rho_i \approx 0.56$ with a half-
width of 0.32; therefore, these measurements correspond
to magnetic fluctuation power at $k\rho_i \approx 0.56 \pm 0.32$.

The upper panel of Fig. 1 shows the distribution of
measurements of proton temperature anisotropy ($T_\perp/T_\parallel$)
against parallel proton plasma beta $\beta_\parallel$; this distribution
shows the striking signatures of the regulation of the
anisotropy by instabilities. These proton measurements
are a subset of those used by Kasper *et al.* [10]; here, we
include only proton measurements at times when there also
exist good measurements of $\delta\vec{B}$. Dotted lines (on all four
panels) show the instability thresholds for the mirror in-
stability at $T_\perp/T_\parallel > 1$ [Eq. (1) with $(a, b, \beta_0) =
(0.77, 0.76, -0.016)$] and the oblique firehose instability
at $T_\perp/T_\parallel < 1$ [Eq. (1) with $(a, b, \beta_0) = (-1.4, 1.0,
-0.11)$] [11]. The second panel of Fig. 1 shows the average
measured amplitude of the magnetic fluctuations $|\delta\vec{B}|/|\vec{B}|$
in the space of $(\beta_\parallel, T_\perp/T_\parallel)$, as in the upper panel. A
general trend of enhanced fluctuations with larger $\beta_\parallel$ is
clearly visible. Furthermore, the fluctuation amplitude is
enhanced along both the mirror/IC (for $T_\perp/T_\parallel > 1$) and
oblique firehose ($T_\perp/T_\parallel < 1$) thresholds. A simple esti-
mate of the pitch-angle scattering rate ν due to Alfvénic
fluctuations gives $\nu = 1/T_\perp dT_\perp/dt \sim \omega_c\langle(\delta B/B)^2\rangle$. If
the first adiabatic invariant is conserved, then the plasma
is driven towards the instability thresholds at a rate com-
parable to the solar wind expansion rate v_{sw}/R, where R is
1 AU. The condition that the pitch-angle scattering be
fast enough to constrain the anisotropy then requires
$\langle\delta B/B\rangle \gtrsim (v_{sw}/\omega_c R)^{1/2} \sim 10^{-3}$, which is the case near
the thresholds and at high β in the second panel of Fig. 1.
This is the principal result of this study.

The third panel of Fig. 1 shows the magnetic compressibility $\delta B_\parallel^2/(\delta B_\parallel^2 + \delta B_\perp^2)$, which is enhanced to values of ~ 0.3 for compressive solar wind ($T_\perp/T_\parallel > 1$) with $\beta_\parallel \gtrsim 1$, as would be expected for the mirror instability. The compressibility becomes smaller for $\beta_\parallel < 1$, which is consistent with the Alfvén ion cyclotron mode; however, the power continues to be bounded by the mirror threshold. Linear mirror instability calculations [15] for $T_\perp/T_\parallel > 1$ predict values of the magnetic compressibility between 0.8 and 1; therefore, our measurements suggest a mixture of waves. Furthermore, it is interesting to note that the typical value of the magnetic compressibility away from the thresholds is small ~ 0.1. The existence of (compressive) magnetosonic or whistler branch waves at short wavelengths [17] would seem to imply larger values of magnetic compressibility. If compressive waves are present, they are likely to be highly mixed with Alfvénic fluctuations, so as to give a small average compressibility.

The bottom panel of Fig. 1 shows the average collisional "age" in each ($\beta_\parallel$, $T_\perp/T_\parallel$) bin; the collisional age τ is defined as $\tau = \nu_{pp} L/\upsilon_{\rm sw}$, the Coulomb proton-proton collision frequency ν_{pp} multiplied by the transit time from the Sun to 1 AU and is an estimate of the number of binary collisions in each plasma parcel during transit from the Sun to the spacecraft. It is interesting, however obvious, that the more collisional plasma is more isotropic; away from $T_\perp/T_\parallel \approx 1$, the plasma is relatively collisionless. It has been shown recently [18] that collisional age organizes solar wind instabilities better than the traditional distinction of "fast" and "slow" wind.

Figure 2 shows the magnetic fluctuations data $|\delta B|$ unnormalized by B. Linear instability thresholds associate with the mirror, ion cyclotron (AIC), and oblique firehose instabilities [11] are overlaid. It is interesting to note that, as found by Hellinger et al. [11], the oblique firehose and the mirror instabilities appear to constrain the observed distribution of data, not the ion cyclotron nor parallel firehose instabilities (in spite of a larger growth rate); this may be because both the mirror and oblique firehose are non-propagating instabilities. The regions of enhanced magnetic fluctuations, near the mirror and oblique firehose thresholds, also correspond to measurements of enhanced proton temperature published elsewhere [19]. It is unclear if this indicates plasma heating due to anisotropy instabilities, in addition to pitch-angle scattering, or if the "younger" (less collisional) plasma is merely hotter than average.

Figure 3 shows histograms of the fluctuation amplitude squared $|\delta B|^2$ in bins of collisional age; the white dots show the most probable value. The overall magnetic fluctuation power δB^2 is a function of the collisional age, with the magnetic power weaker by a factor of ~ 100 for more collisional plasma. This effect is a proxy for the temperature anisotropy: collisional plasma is more isotropic and, therefore, further from the instability thresholds. This
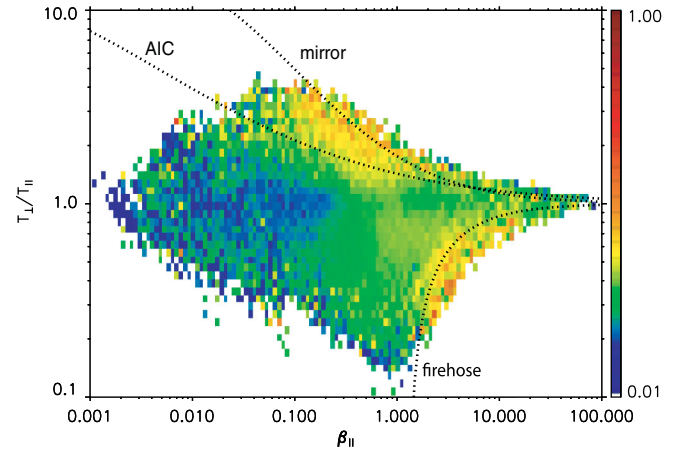

FIG. 2 (color).   The magnitude of magnetic fluctuations $|\delta B|$ averaged into bins of $T_\perp/T_\parallel$ vs $\beta_\parallel$. Enhanced power exists well away from the thresholds, as expected. The regions of enhanced δB corresponds to the enhanced proton heating in Liu et al. (2006).

underscores the important point that the power spectral density (PSD) of magnetic fluctuation power near 1 Hz in the solar wind is modified by these local instabilities. Previous studies of the PSD of short wavelength solar wind turbulence have not accounted for this and should be reexamined [20–24]. If the $|\delta B|^2$ values in Fig. 3 are divided by the measurement bandwidth (approximately 5–10 Hz depending on sample rate), they can be compared to power spectral density (PSD) measurements published previously (over the bandwidth of 0.3 to 11 Hz), noting that the power is dominated by the amplitude at the lowest frequencies (0.3 Hz). A log-log fit to the most probable
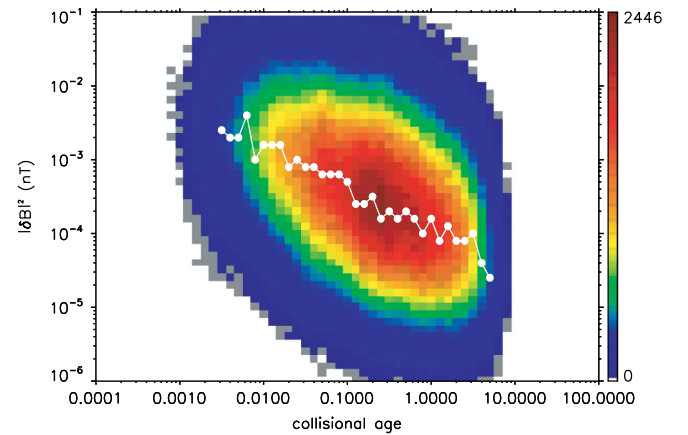

FIG. 3 (color).   Magnetic fluctuation amplitude $|\delta B|^2$ as a function of the collisional age; the white dots are the most likely value of $|\delta B|^2$ in each age bin. Magnetic fluctuations near the proton gyroradius ($k\rho \approx 1/2$) are suppressed in more collisional plasma. Coulomb collisions maintain the isotropy of the protons, which then remain far from the instability thresholds. Note that this corresponds to a factor of 100 suppression of magnetic power δB^2 over the full range of collisionality.
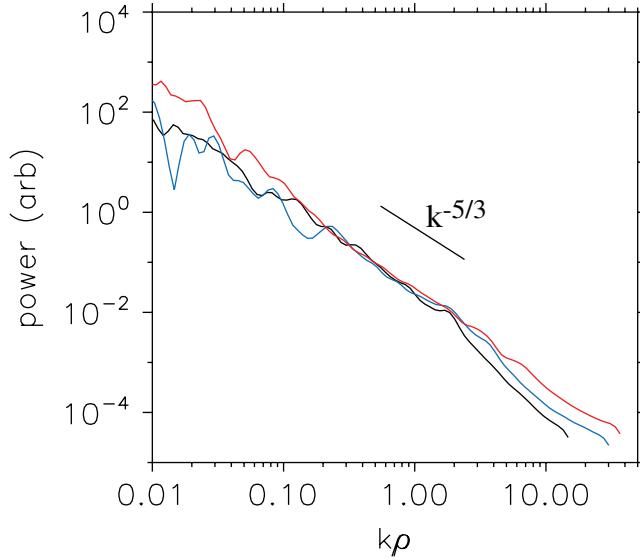
FIG. 4 (color).   Wavelet power spectra of magnetic fluctuations
at three different time intervals corresponding to perpendicu-
lar anisotropy $T_\perp/T_\parallel = 2.2$, $\beta_\parallel = 0.2$ (red trace), parallel an-
isotropy $T_\perp/T_\parallel = 0.5$, $\beta_\parallel = 1.9$ (blue trace), and isotropic pro-
tons $T_\perp/T_\parallel = 1$, $\beta_\parallel = 0.7$ (black trace). The spectra are plotted
against $k\rho$ and have been scaled to the same average value over
the interval $k\rho \in (0.2, 1.0)$, as described in the text. A solid
black line with scaling $k^{-5/3}$ is shown. The interval above $k\rho \approx$
$1/2$ corresponds to the statistical data shown in Figs. 1 and 2.

values in Fig. 3 gives a relationship $|\delta B|^2 \approx 10^{-4}\tau^{-0.57}$,
where $\tau = \nu_{pp}L/v_{\rm sw}$ is the collisional age.

   Figure 4 shows wavelet power spectral density for three
distinct time intervals; these spectra are shown plotted
against $k\rho_i$ assuming Taylor's hypothesis ($\omega = kv_{\rm sw}$)
and using the local values of $v_{\rm sw}$, $v_{\rm th}$, and $\omega_{\rm ci}$ and scaling
the spectra to have similar power over the range $k\rho_i \in$
$(0.2, 1.0)$. The black trace in Fig. 4 shows the magnetic
power from an interval of isotropic plasma ($T_\perp/T_\parallel, \beta_\parallel) \approx$
$(1, 0.7)$, the red trace is data from an interval of perpen-
dicular anisotropy ($T_\perp/T_\parallel, \beta_\parallel) \approx (2.2, 0.2)$, and the blue
trace from an interval of parallel anisotropy ($T_\perp/T_\parallel, \beta_\parallel) \approx$
$(0.5, 1.9)$. Wave numbers below $k\rho_i \approx 0.2$ are aliased by
the Morlet wavelet transform and are unreliable. Although
the inertial range, where the power is proportional to $k^{-5/3}$
(shown by a solid black line in Fig. 4), can be made to
agree, the nature of the short wavelength spectrum above
$k\rho_i \approx 1$ varies between spectra. While this result is not
statistical, nor is it surprising given the clear organization
of the magnetic fluctuation power in Fig. 1, it begs a
reexamination of "dissipation range" turbulence. Future
observational studies of turbulent dissipation and second-

ary (kinetic Alfvén wave) cascades should attempt to
understand the role of these local instabilities, which may
confuse the interpretation of solar wind magnetic power
spectra.

[1] G. F. Chew, M. L. Goldberger, and F. E. Low, Proc. R. Soc.
     A **236**, 112 (1956).
[2] A. Eviatar and M. Schulz, Planet. Space Sci. **18**, 321
     (1970).
[3] A. A. Schekochihin, S. C. Cowley, R. M. Kulsrud, G. W.
     Hammett, and P. Sharma, Astrophys. J. **629**, 139 (2005).
[4] P. Sharma, G. W. Hammett, E. Quataert, and J. M. Stone,
     Astrophys. J. **637**, 952 (2006).
[5] P. Sharma, E. Quataert, G. W. Hammett, and J. M. Stone,
     Astrophys. J. **667**, 714 (2007).
[6] E. E. Scime, P. A. Keiter, M. M. Balkey, R. F. Boivin, J. L.
     Kline, M. Blackburn, and S. P. Gary, Phys. Plasmas **7**,
     2157 (2000).
[7] S. P. Gary, R. M. Skoug, J. T. Steinberg, and C. W. Smith,
     Geophys. Res. Lett. **28**, 2759 (2001).
[8] B. J. Anderson, S. A. Fuselier, S. P. Gary, and R. E.
     Denton, J. Geophys. Res. **99**, 5877 (1994).
[9] T. D. Phan, D. E. Larson, R. P. Lin, J. P. McFadden, K. A.
     Anderson, C. W. Carlson, R. E. Ergun, S. M. Ashford, M.
     McCarthy, and G. Parks et al., Geophys. Res. Lett. **23**,
     1279 (1996).
[10] J. C. Kasper, A. J. Lazarus, and S. P. Gary, Geophys. Res.
     Lett. **29**, 1839 (2002).
[11] P. Hellinger, P. M. Travnciek, J. C. Kasper, and A. J.
     Lazarus, Geophys. Res. Lett. **33**, L09101 (2006).
[12] S. P. Gary and M. A. Lee, J. Geophys. Res. **99**, 11297
     (1994).
[13] K. W. Ogilvie et al., Space Sci. Rev. **71**, 55 (1995).
[14] R. P. Lepping et al., Space Sci. Rev. **71**, 207 (1995).
[15] D. Krauss-Varban, N. Omidi, and K. B. Quest, J. Geophys.
     Res. **99**, 5987 (1994).
[16] P. Goldreich and S. Sridhar, Astrophys. J. **438**, 763 (1995).
[17] S. Saito, S. P. Gary, H. Li, and Y. Narita, Phys. Plasmas **15**,
     102305 (2008).
[18] J. C. Kasper, A. J. Lazarus, and S. P. Gary, Phys. Rev. Lett.
     101, 261103 (2008).
[19] Y. Liu, J. D. Richardson, J. W. Belcher, and J. C. Kasper,
     J. Geophys. Res. **111**, A01102 (2006).
[20] R. J. Leamon, C. W. Smith, N. F. Ness, and H. K. Wong,
     J. Geophys. Res. **104**, 22331 (1999).
[21] S. D. Bale, P. J. Kellogg, F. S. Mozer, T. S. Horbury, and
     H. Reme, Phys. Rev. Lett. **94**, 215002 (2005).
[22] O. Alexandrova, V. Carbone, P. Veltri, and L. Sorriso-
     Valvo, Astrophys. J. **674**, 1153 (2008).
[23] T. S. Horbury, M. Forman, and S. Oughton, Phys. Rev.
     Lett. **101**, 175005 (2008).
[24] J. J. Podesta, Astrophys. J. **698**, 986 (2009).